AD_____

Award Number: W81XWH-11-1-0332

TITLE: High-Resolution Large-Field-of-View Ultrasound Breast Imager

PRINCIPAL INVESTIGATOR: Patrick LaRiviere, Ph.D.

CONTRACTING ORGANIZATION: University of Chicago
Chicago, Illinois 60637-5418

REPORT DATE: June 2013

TYPE OF REPORT: Annual

PREPARED FOR: U.S. Army Medical Research and Materiel Command
Fort Detrick, Maryland 21702-5012

REPORT DOCUMENTATION PAGE

Form Approved
OMB No. 0704-0188

1. REPORT DATE	2. REPORT TYPE	3. DATES COVERED
June 2013	Annual	1 June 2012 – 31 May 2013

4. TITLE AND SUBTITLE

High Resolution Large Field of View Ultrasound Breast Imager

5a. CONTRACT NUMBER

5b. GRANT NUMBER
W81XWH-11-1-0332

5c. PROGRAM ELEMENT NUMBER

6. AUTHOR(S)

Patrick LaRiviere, Ph.D.

E-Mail: pjlarivi@uchicago.edu

5d. PROJECT NUMBER

5e. TASK NUMBER

5f. WORK UNIT NUMBER

7. PERFORMING ORGANIZATION NAME(S) AND ADDRESS(ES)

University of Chicago
Chicago, Illinois 60637-5418

8. PERFORMING ORGANIZATION REPORT NUMBER

9. SPONSORING / MONITORING AGENCY NAME(S) AND ADDRESS(ES)
U.S. Army Medical Research and Materiel Command
Fort Detrick, Maryland 21702-5012

10. SPONSOR/MONITOR'S ACRONYM(S)

11. SPONSOR/MONITOR'S REPORT NUMBER(S)

12. DISTRIBUTION / AVAILABILITY STATEMENT
Approved for Public Release; Distribution Unlimited

13. SUPPLEMENTARY NOTES

14. ABSTRACT

In this work, we are seeking to construct and test the first practical full-field transmission ultrasound breast imaging system. The system will have a large field-of-view capable of producing 2D images of the entire breast in near real-time. Because it uses a fixed imaging geometry that does not involve scanning, it will also circumvent the operator-dependence of conventional ultrasound imaging methods. The compact vertical design mimics the form factor of mammography systems and would provide a basis for later incorporation of an x-ray source and detector, which would allow for routine dual-modality x-ray and acoustic imaging for screening and diagnosis. If successful, this work will provide the basis for a dual-modality ultrasound and mammography imaging system that could help improve early detection of breast cancer, especially in young women with dense breasts, which are often not well visualized mammographically. It would also help reduce false positives, which add to the expense and anxiety associated with current approaches to breast cancer screening.

15. SUBJECT TERMS
Breast imaging, acoustomammography, breast cancer.

16. SECURITY CLASSIFICATION OF:			17. LIMITATION OF ABSTRACT	18. NUMBER OF PAGES	19a. NAME OF RESPONSIBLE PERSON
a. REPORT	b. ABSTRACT	c. THIS PAGE			USAMRMC
U	U	U	UU	22	19b. TELEPHONE NUMBER *(include area code)*

Table of Contents

Page

Annual Report for W81XWH-11-1-0332
PI: Patrick La Riviere

Note: This report builds on the year 1 report. New sections are indicated with a marginal line.

INTRODUCTION:

In this work, we are seeking to construct and test the first practical full-field transmission ultrasound breast imaging system. The system will have a large field-of-view capable of producing 2D images of the entire breast in near real-time. Because it uses a fixed imaging geometry that does not involve scanning, it will also circumvent the operator-dependence of conventional ultrasound imaging methods. The compact vertical design mimics the form factor of mammography systems and would provide a basis for later incorporation of an x-ray source and detector, which would allow for routine dual-modality x-ray and acoustic imaging for screening and diagnosis.If successful, this work will provide the basis for a dual-modality ultrasound and mammography imaging system that could help improve early detection of breast cancer, especially in young women with dense breasts, which are often not well visualized mammographically. It would also help reduce false positives, which add to the expense and anxiety associated with current approaches to breast cancer screening.

BODY:

Year 1 Summary: We have made substantial progress in this first year of the project. Most tasks in the original Statement of Work for year 1 have been completed on schedule. The only delay has been in the optimization, fabrication, and acceptance testing of the lenses, which we had scheduled to complete within 9 months and is just now wrapping up in the 13th month. This arose mainly from the need to alter our original design from a refraction-based system to a reflection-based system, due to unacceptably high levels of acoustic attenuation predicted in the refraction-based system.

Year 2 Summary: We fell much further behind schedule this year due to delays in receipt of the lenses and delays involved in designing and fabricating appropriate adjustable lens mounts that allow for rotation, tilt, and translation. We are very close to having a complete system now, which will allow for final testing in the no-cost extension period. We also explored a new direction related to using multi-frequency acquisitions to characterize lesion size.

Aim 1:To design and construct a high-resolution, large field of view ultrasound breast imager by combining a super high-resolution AO sensor and a large aperture acoustic lens.

Task 1: Design, fabricate, and test sound source
1.a. Simulate acoustic propagation from array of 9 2.7" elements to confirm suitability of design choice (U of C; mos. 1-2).

We have developed theory and software necessary to simulate the acoustic field emanating from square transducer elements. In brief, we made use of standard Rayleigh-Summerfield diffraction theory and the angular spectrum decomposition to develop expressions for the field propagating from a rectangular

piston-like transducer. By the linearity of the resulting equations, we can use superposition to determine the field produced by an array of square or rectangular transducers.

The details are provided in Appendix A, but the key results are shown in Fig 1 below, which illustrates the normalized in-plane acoustic intensity distribution at a distance 2 inches from a 3” by 3” square transducer piston operating at a CW frequency of 3.35 MHz. The figure shows both a surface plot and a color mapped intensity distribution.

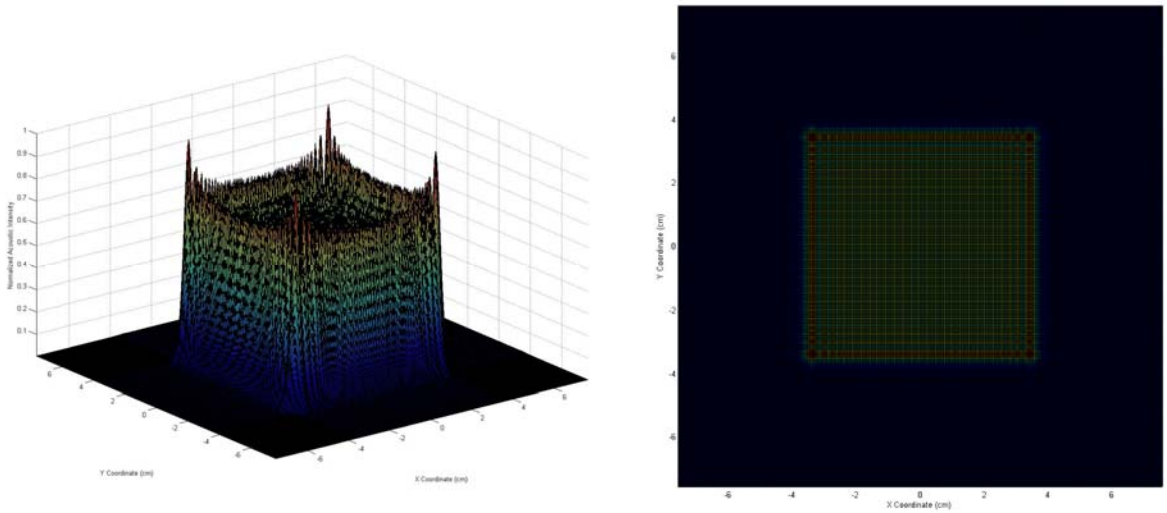

Figure 1: (Left) The normalized in-plane acoustic intensity distribution for a 3” by 3” square transducer piston operating at a CW frequency of 3.35 MHz. The pressure field intensity is depicted in the plane parallel to the transducer surface at a distance of 2”, and a background medium of water has been assumed. We note that the square modulus of the acoustic pressure field is plotted. (Right) This figure presents the same information as the left plot but shows the spatial distribution of acoustic intensity looking at the plane of interest head-on. For a planar detector positioned 2” from the transducer surface, one would expect to observe this type of diffraction pattern for an image acquired with no scattering object present.

1.b. Fabricate source array (Santec; mos. 2-3)

A large-area sound source has been designed and fabricated with four 4 MHz, 3”x3” size elements. The original plan called for working at 3.35 MHz, but technical difficulties necessitated a change to 4 MHz, which should not affect any of the properties of the planned system. A quarter-wavelength acoustic matching layer was provided to allow efficient operation in water. Each element was electrically tuned to match to the 50-Ohm impedance of an RF Amplifier powered by a 4.0 MHz electrical signal from a digital function generator. An RF power splitter was also designed and built to distribute RF power equally to all 4 elements of the sound source. First-level software was also developed to allow digital

control of acoustic power output of the sound source. The current design is being extended to build a larger source to cover the 8"x8" field area.

1.c Test source and compare with simulation results (U of C; mos. 3-4)

Our preliminary comparisons indicate good agreement between the real and simulated fields. More detailed comparison work is ongoing.

Task 2: Fabricate and test AO sensor
2.a Fabricate 1" X 1" AO sensor (Santec; mos. 4-5)

At least three 4 MHz AO sensors have been built. We were able to overcome some technical challenges and build even larger sensors than originally planned. The detection area of each sensor was at least 2"x2". The acoustic detection sensitivity of these sensors was found to be in the milliWatt/cm^2 range. The angular acceptance of the AO sensor is at least 20^o about normal incidence condition. The acoustic detection sensitivity was quite dependent on the acoustic beam angle, and might impact image quality. However, this needs to be studied using the acoustic lens (or mirrors) being designed so that if needed, the AO sensor design can be change to minimize the angular effect. The milliWatt/cm^2 range acoustic detection sensitivity of the AO sensor should be adequate to allow us to operate the Breast Imager below the FDA specified safety standard.

2.b Test resolution and sensitivity of AO sensor (U of C; mos. 5-6)

We sought to characterize the spatial resolution of the prototype transmission ultrasound imaging system by deriving estimates for the edge spread function (ESF), the line spread function (LSF), and the pre-sampled modulation transfer function (MTF) of the system. We also sought to characterize the noise properties of the prototype transmission ultrasound imaging system by determining an estimate for the noise power spectrum (NPS) of the system.

Spatial Resolution Analysis
The spatial resolution analysis was performed using the angled edge technique originally proposed by Reichenbach *et al*. [1], in which use of a small (~ 3^o) edge angle permits finer sampling of the system ESF than the pixel pitch of a digital detector, thus minimizing the possibility of MTF aliasing. A transmission ultrasound image of a slightly angled knife edge was acquired with temporal averaging to reduce noise. A segment of the knife edge image is shown in Figure 2. Each row of pixels in Figure 2 provided a shifted sample of the knife edge. The individual rows were spatially registered by estimating the edge position within

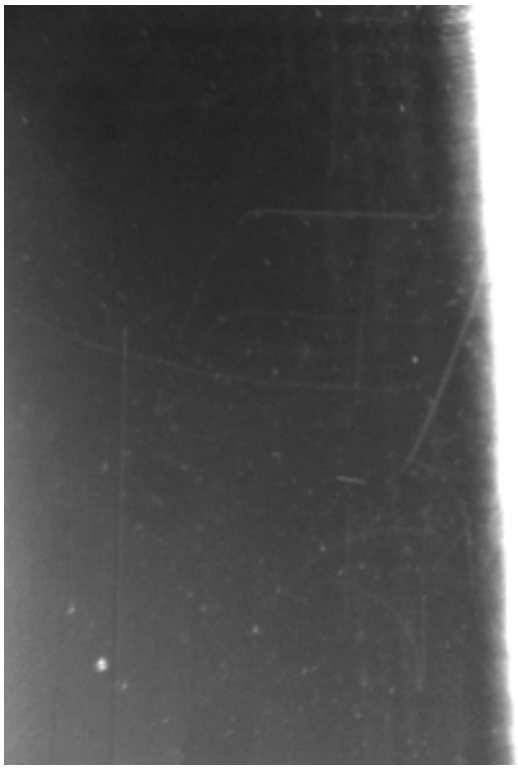

Figure 2: Image of the knife edge used to compute the pre-sampled MTF of the imaging system. The image was acquired using a peak transducer voltage of 0.7 V. Continuous frequency sweeping of 3.25-3.45 MHz at 100 MHz/s was also employed to minimize speckle artifacts due to acoustic wave coherence.

After shifting each row of pixel values by the estimated edge location, the spatially registered data points were averaged over .0625-mm intervals to obtain an estimate of the system ESF. Following the work of Boone and Seibert [2], the measured ESF data was fit to a combined error function and exponential fit of the form

$$\mathrm{ESF}(x) = \mathbf{a}\,\mathrm{sgn}(x - x_0)\left\{1 - \exp\left(-\mathbf{b}|x - x_0|\right)\right\} + \mathbf{c}\left\{\mathrm{erf}\left(\sqrt{\mathbf{d}}(x - x_0)\right)\right\} + \mathbf{e}.$$

Analytic estimates for the normalized system LSF and MTF were determined from the fit parameters ***a****,* ***b****,* ***c****,* ***d****,* ***e****, and* x_0 *according to the relations*

$$\mathrm{LSF}(x) = \frac{1}{2(\mathbf{a}+\mathbf{c})}\left[\mathbf{ab}\exp\left(-\mathbf{b}|x - x_0|\right) + 2\mathbf{c}\sqrt{\frac{\mathbf{d}}{\pi}}\exp\left(-\mathbf{d}(x - x_0)^2\right)\right].$$

$$\mathrm{MTF}(f) = \frac{1}{\mathbf{a}+\mathbf{c}}\left[\mathbf{c}\exp\left(-\frac{\pi^2 f^2}{\mathbf{d}}\right) + \mathbf{a}\left(1 + \frac{4\pi^2 f^2}{\mathbf{b}^2}\right)^{-1}\right].$$

Spatial Resolution Analysis Results

Figure 3 presents the measured ESF data points with overlaid exponential-error function regression model. The statistics of the computed fit are also provided.

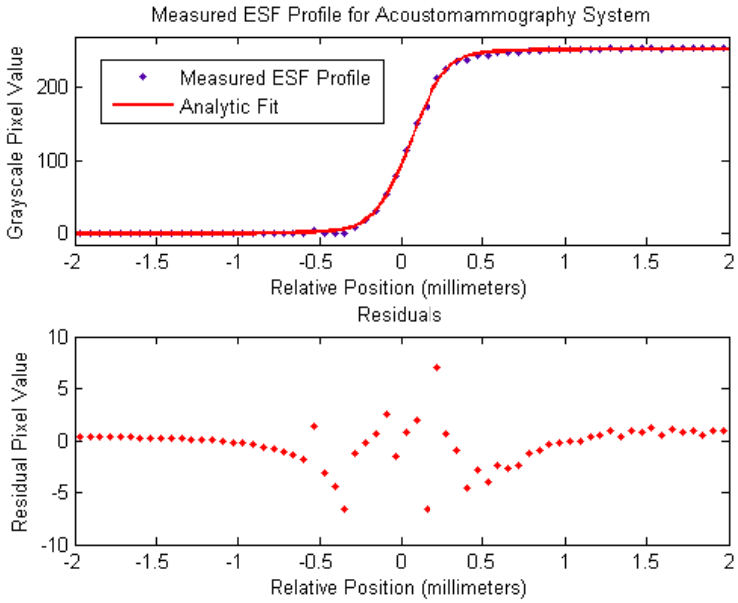

Regression Statistics

Fit Coefficients:

a = 17.77

b = 3.22 mm^{-1}

c = 108.9

d = 17.4975 mm^{-2}

e = 126.3

x_0 = 0.05298 mm

Goodness of fit:

r^2 = 0.9999

RMSE: 1.426

Figure 3: Measured ESF data and analytic regression model with residual subplot. The r^2 value for the regression curve is 0.9999, and the root-mean-square error (RMSE) is only 1.15% of the mean measured ESF value. These statistics indicate that the combined exponential-error function regression model provides an excellent fit to the measured data.

Figure 4 shows the normalized analytic LSF and the analytic pre-sampled MTF derived from the regression equation used to fit the ESF data in Figure 6.

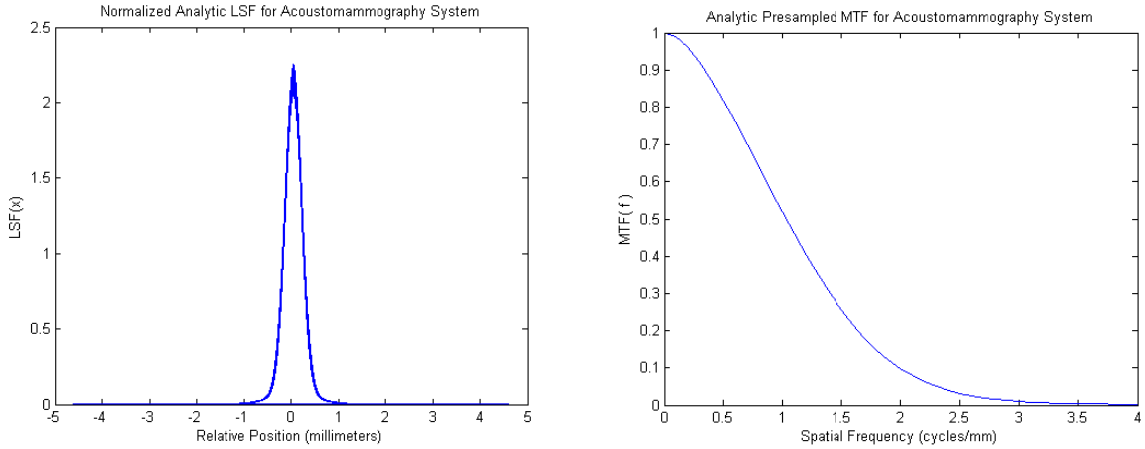

Figure 4: The normalized analytic LSF and the analytic pre-sampled MTF for the transmission ultrasound imaging system. These curves were obtained from the fitting parameters of the combined exponential-error function regression model used to fit the measured ESF data. The full-width-at-half-maximum (FWHM) of the system LSF indicates an approximate spatial resolution of 400 microns.

The FWHM of the analytic LSF was calculated to be 0.3997 millimeters, indicating an approximate spatial resolution of 400 microns for the prototype transmission ultrasound imaging system. The analytic curve for the pre-sampled MTF shows a typical Gaussian form. The curve is equal to unity at zero spatial frequency and falls off smoothly to nearly zero at the system Nyquist frequency (3.79 cycles/mm).

Noise Analysis

The NPS of the imaging system was determined by acquiring 25 detector flood images using the same transducer settings for each acquisition. One such image is included in Figure 5.For each flood image, a subsection of the total image matrix was extracted over which the detector illumination appeared highly uniform. The NPS of each subsection was computed by subtracting the mean pixel value <PV> and computing the square modulus of the two-dimensional discrete Fourier transform of the resulting matrix. In the continuum,

$$\mathrm{NPS}(\mathbf{f}) = \left| \int_{-\infty}^{\infty} \int_{-\infty}^{\infty} \left[\mathrm{PV}(\mathbf{r}) - \langle \mathrm{PV} \rangle \right] e^{-j2\pi \mathbf{f}\cdot\mathbf{r}} d^2\mathbf{r} \right|^2 .$$

The 25 separately computed noise power spectra were averaged to obtain a mean estimate for the NPS of the system. This estimate was normalized by its largest amplitude component and plotted as a two-dimensional function of spatial frequency **f**.

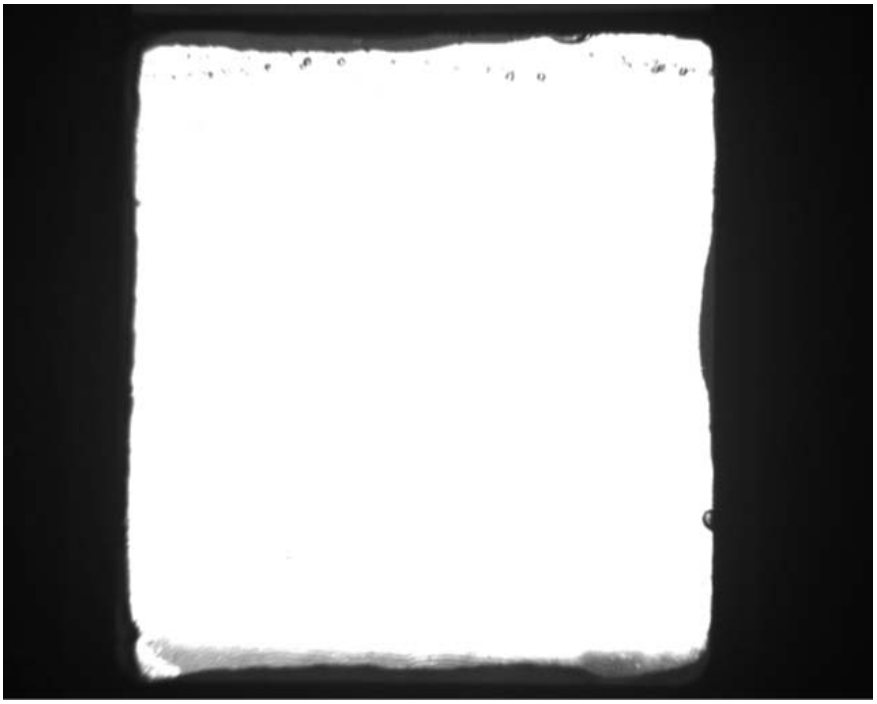

Figure 5: Example of one of the detector flood images used to estimate the NPS of the imaging system. The image shows highly uniform illumination of the AO detector field of view. A peak transducer voltage of 2.6 V and frequency sweeping of 3.25-3.45 MHz at a rate of 100 MHz/s were used because of the uniform detector illumination provided by these settings

Figure 6 presents an estimate of the two-dimensional NPS of the imaging system as a surface plot. The height of the NPS indicates the noise power contained per unit frequency bandwidth at each corresponding spatial frequency. It can be seen that significant noise power is contained at lower spatial frequencies near zero frequency. The NPS amplitude falls steadily when moving toward higher spatial frequencies.

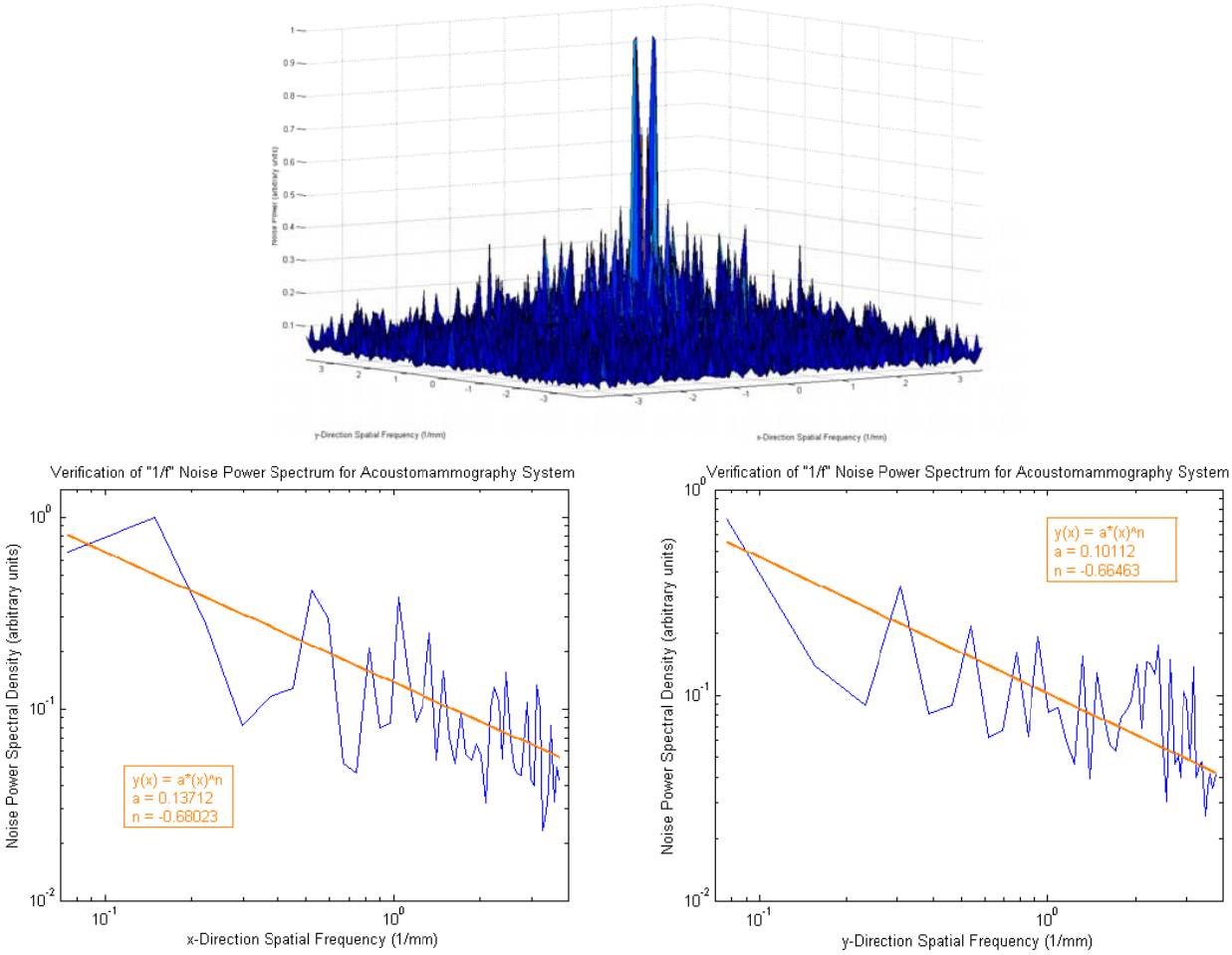

Figure 6: Surface plot of the two-dimensional NPS of the transmission ultrasound imaging system. The lower two graphs show single slices taken through the NPS surface plot along the x- and y-spatial frequency axes. These slices are plotted on log-log axes to demonstrate the presence of 1/f noise in the imaging system.

The lower two plots in Figure 6 show single slices of the NPS taken along the *x*-spatial frequency and *y*-spatial frequency axes. For these graphs, the NPS is plotted on log-log axes.These slices are well fit by power law regression models, which appear as straight lines on the log-log plots. The characteristic exponent values of the regression models are 0.680 mm^{-1} and 0.665 mm^{-1} for the *x*- and *y*-directions, respectively. This type of behavior is ubiquitous in nature and is termed "1/*f* noise." It is caused by random fluctuations in the solid-state circuit elements comprising most electronic devices.

Task conclusions

- Though the intrinsic spatial resolution of the AO detector is itself very high (~ 10^{-9} meters) the spatial resolution of the imaging system is substantially reduced by the pixelation of the digital camera used to record the display of the AO detector for image processing and storage. The measured resolution is 400 microns.
- The noise present in the imaging system is primarily electrical in nature, as evidenced by the $1/f$ noise behavior observed in the system NPS in both the x- and y-spatial directions.

Multifrequency acquisition for lesion size determination

With a noise model in hand, we began to investigate a new direction involving the potential for acquiring images at two frequencies and exploiting the frequency dependence of ultrasonic attenuation to perform lesion identification and size estimation.

Purpose: To investigate the feasibility of using a limited number of multispectral transmission ultrasound images acquired with a novel full-field liquid crystal ultrasonic detector to estimate the sizes of cystic and malignant breast lesions.

Methods: In our prototype ultrasound imaging system, a high-resolution liquid crystal detector measures the intensity of the acoustic field transmitted through the compressed breast. Projection images can be acquired at multiple transducer frequencies with several monochromatic sources. Assuming normal breast parenchyma containing either a simple breast cyst or infiltrating duct carcinoma, image data acquired at two or more transducer frequencies can potentially be used to estimate the size of the lesion present. The presence of electrical Gaussian noise precludes an exact lesion thickness determination; the lesion thickness can only be estimated with some uncertainty. We have used estimation theory to derive the Cramer-Rao lower bound on the uncertainty of the thickness estimate for cystic and malignant lesions of variable sizes.

Results: For a 1-cm simple breast cyst and SNR of 50, an uncertainty in the estimated cyst thickness of 0.1641 cm can be obtained using two transmission ultrasound breast images acquired with transducer frequencies of 6 and 7.997 MHz. For a malignant breast lesion of the same size and SNR of 50, an uncertainty in the lesion thickness estimate of 0.197 cm can be obtained using two breast images acquired with transducer frequencies of 5 MHz and 5.462 MHz. In general, the lower bound on the precision of the thickness estimate is found to improve with increasing SNR and lesion size. Typical results are shown in Fig 7.

Conclusion: For the cases considered, the Cramer-Rao lower bound on the precision of the thickness estimate is significantly less than the actual lesion thickness. The precision of the thickness estimate can potentially be improved by using lower transducer frequencies, although diffraction artifacts might then become prohibitive.

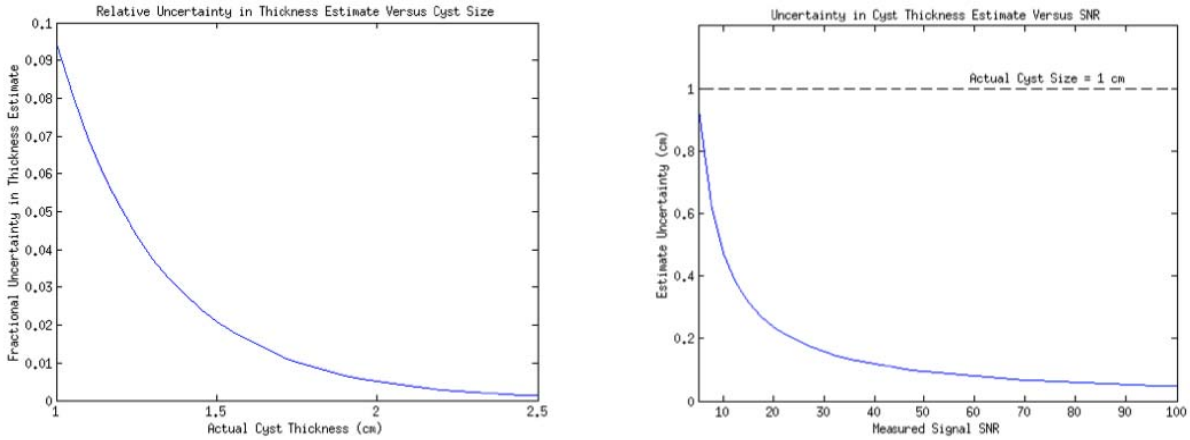

Figure 7: (Left) Relative precision of thickness estimate vs cyst size for SNR of 50. (Right) Uncertainty in cyst thickness estimate versus SNR.

Task 3: Incorporate video camera

3.a. Incorporate the new video camera with source and AO sensor (no lens yet) and test resolution and sensitivity (U of C; mo. 6)

We have not yet incorporated the new video camera. The results above were acquired with the original video camera. Adding the video camera will be a simple modification to incorporate along with the lenses.

Task 4: Design, fabricate, and test acoustic lens

4.a. Determine final lens specifications based on simulation studies of whole system (U of C; mos 1-3)

Our initial plan was to fabricate an afocal triplet of acoustic lenses, as shown in Fig. 8.

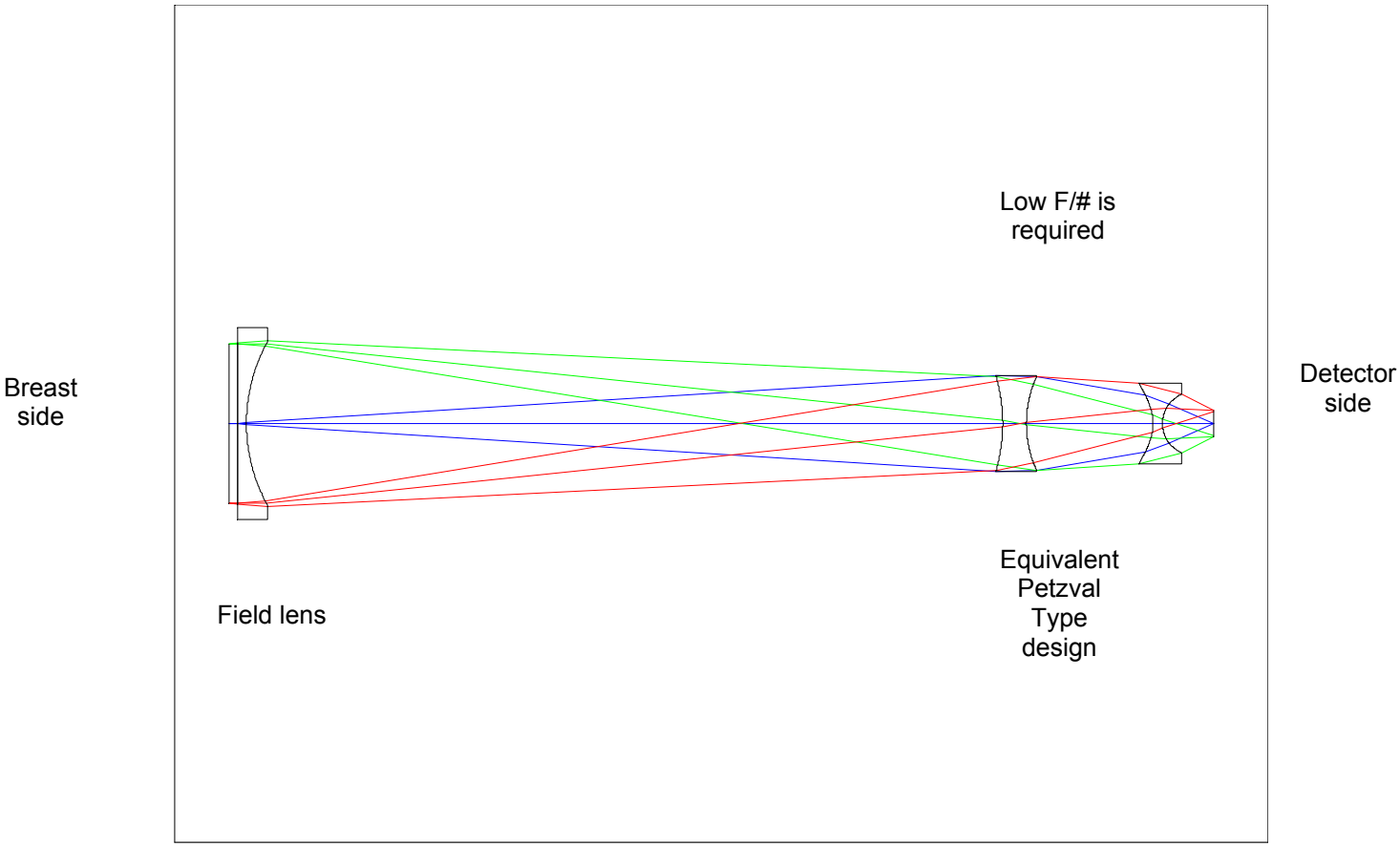

Fig.8: Initial afocal triplet design. The acoustic attenuation in this design would have been too high.

However, initial design and simulation studies showed that because of the fast speed of the lens required (~F/3 or less), the lens thickness variation would have been about ~60 mm which would have caused unacceptable attenuation of the acoustic field.

An alternative single-lens design, shown in Fig. 8, would still have been too thick (56 mm), leading to two or three orders of magnitude of acoustic attenuation. Therefore it was decided to produce a reflective system rather than a refractive lens.

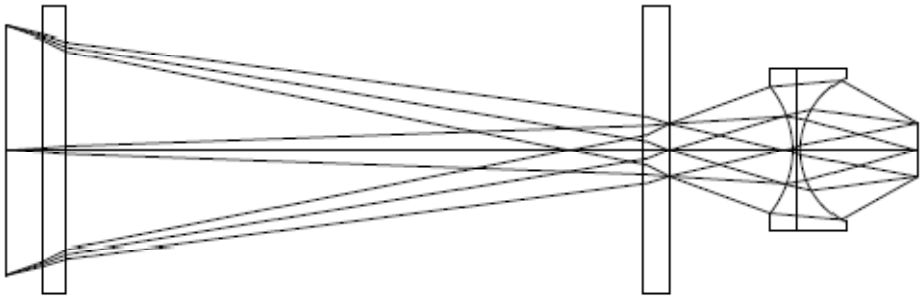

Fig 9: A single-lens design aimed at reducing acoustic attenuation still would have had unacceptable levels of it. We turned instead to a reflection-based system.

4.b. Optimize lens design using Zemax lens design software (U of C/Sasian; mos. 4-6)

We used the Zemax lens design software to optimize the mirror-based system. The schematic of the optimized mirror-based system is shown below in Fig 10

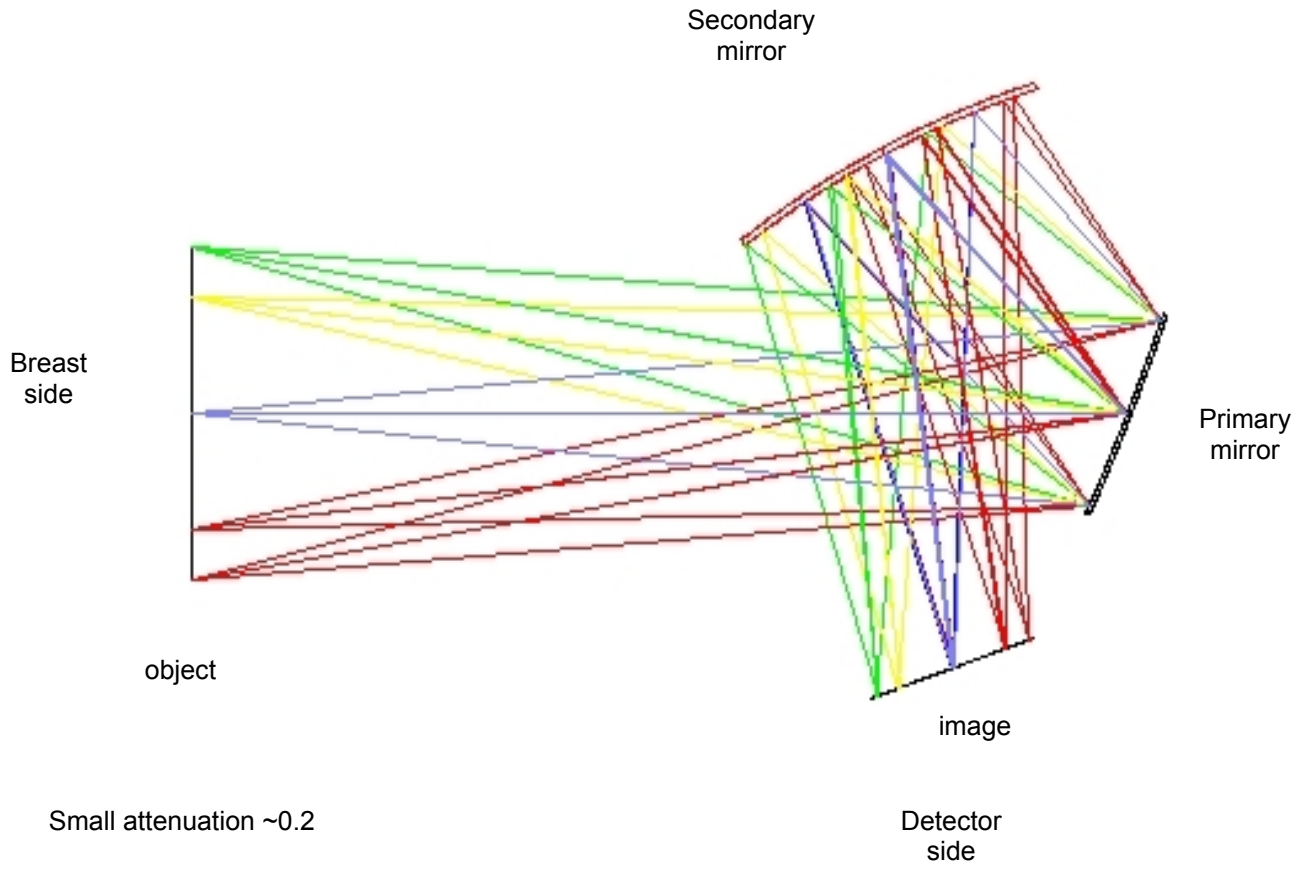

Fig 10: Cross-sectional schematic of the lens-based system.

A three-dimensional rendering is shown in Fig. 11.

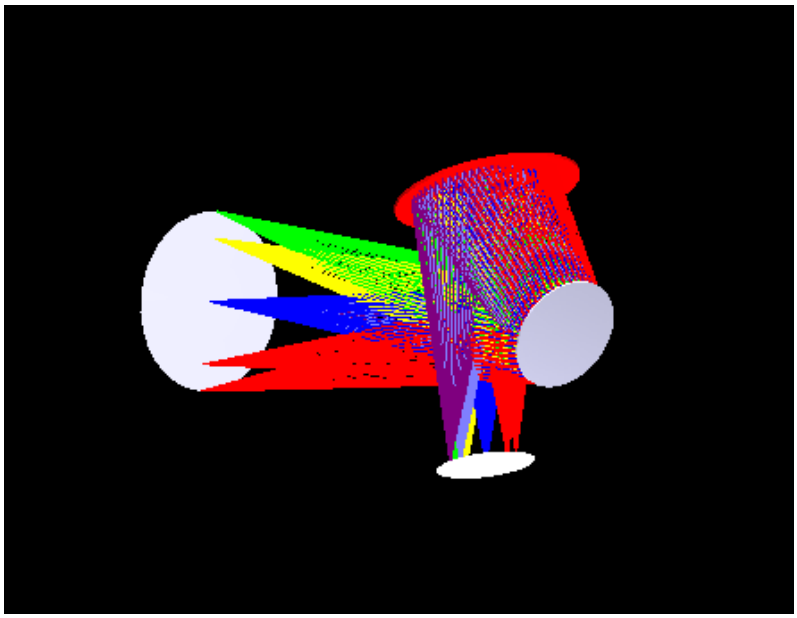

Fig 11: Three-dimensional view of the mirror-based system.

The system characteristics are as follows:

- Length: 600 mm
- Width: 310 mm
- Working F/# = 2.88
- Wavelength: 0.5 mm
- Stop aperture at primary mirror
- Other apertures for stray sound suppression are allowed
- System is plane symmetric in y-z plane
- Magnification 0.5

The primary mirror surface, which is concave, is described by

$$sag = \frac{c\left(x^2 + y^2\right)}{1 + \sqrt{1 - c^2\left(x^2 + y^2\right)}} + Ay^2 + Bx^2 y + Cy^3$$

with parameters

- c =-1/1000 mm
- A=1.555861e-4 mm^{-1}
- B=5.74993e-7 mm^{-2}
- C=5.160419e-7 mm^{-2}
- Diameter = 130 mm

With these specifications, the expected performance is given in the Airy disk diagrams shown in Fig. 12.

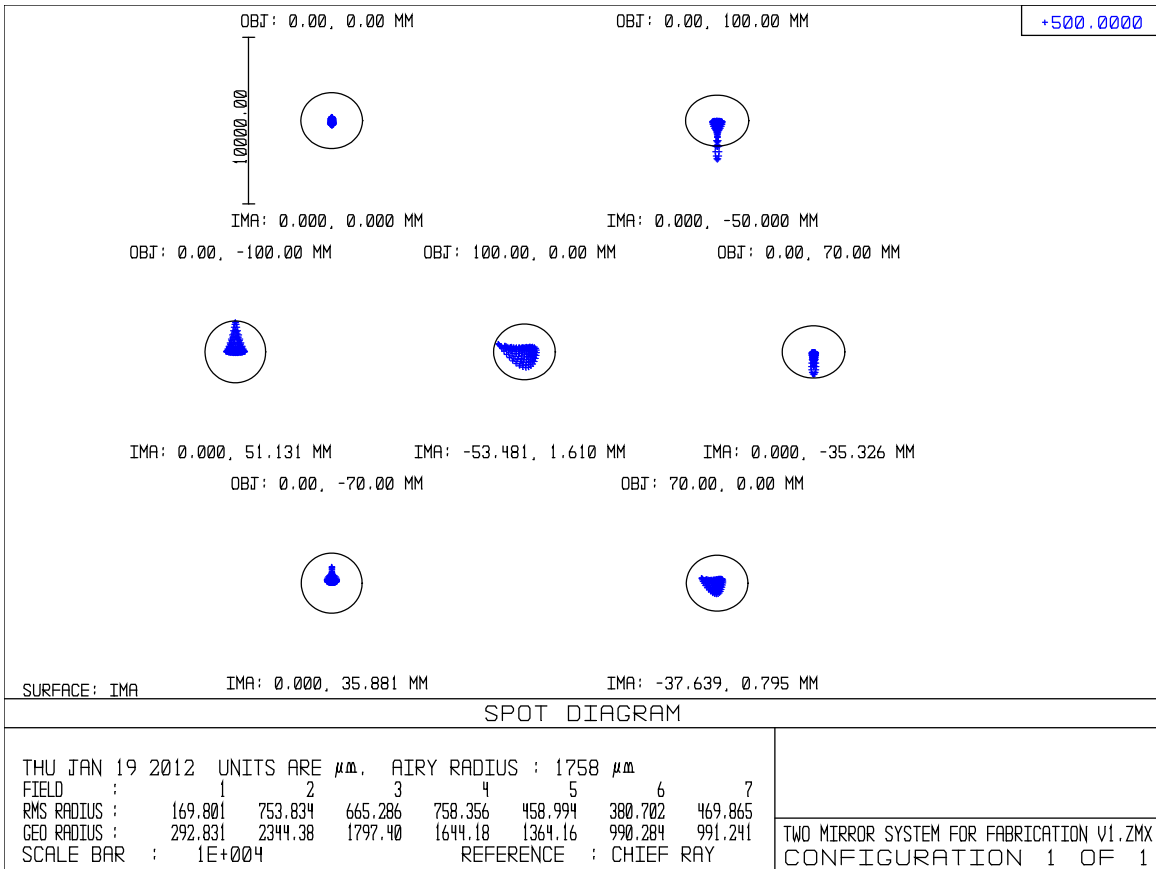

Fig 12: Airy spot diagrams showing expected performance of the lens system.

4.c. Fabricate lens (U of C/Sasian; mos. 7-8)

The lenses have been successfully fabricated by Lam Optics in Tucson, AZ.

4.d. Perform acceptance testing on lens (U of C; mo. 9)

Consultant Jose Sasian personally visited the fabrication facility to observe fabrication and oversaw in-house quality assurance. He performed preliminary acceptance testing before the lenses were sent to the University of Chicago. Final testing will take place during alignment and focusing.

Task 5: Assemble complete system

5.a. Fabricate immersion tank (Santec; mo. 9)

An appropriate immersion tank has been assembled by Santec systems Inc.

5.b. Assemble system (U of C; mo. 10-12)

Assembly of the complete system was delayed by late delivery of the lenses and further slowed by delays in fabricating appropriate adjustable mounts for the acoustic mirrors. Any sort of compound focusing system requires careful positioning and alignment. For optical lenses and mirrors, there are many vendors providing off-the-shelf mounts that allow for fine adjustment and stable positioning. Such mounts are not readily available for the kind of large acoustic mirrors we ended up designing for this

project. Thus for our problem we need a customized solution. The spacings and rotation and tilt angles are given in Fig. 13.

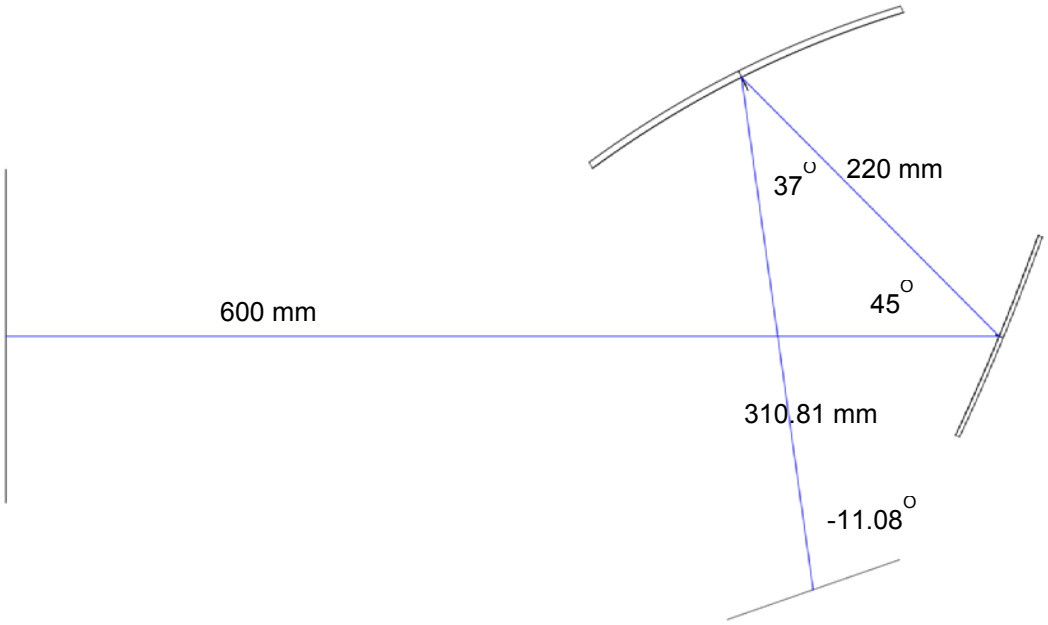

Fig 13: Mirror spacings and angles.

We determined the following specifications for the lens mounts:

Primary mirror:

- Needs to be able to tilt in X and Y ~8 degrees
- Needs to be able to be located in XYZ by ~+/- 5 mm
- Needs to be able to rotate ~+/- 12 degrees
- Select three point mount
- Attach support to mirror back
- Use mirror with toroid and comatic shape

Secondary mirror:

- Needs to be able to tilt in X and Y ~8 degrees
- Needs to be able to be located in XYZ by ~+/- 5 mm
- Select three point mount
- Attach support to mirror back

Sensor:

- Needs to be able to tilt in X and Y ~8 degrees
- Needs to be able to be located in XYZ by ~+/- 5 mm

Suitable mounts have been designed and fabricated and alignment is currently underway using a laser to align mirrors to proper distances, followed by a point source allowing for final alignment as shown in Figs. 14 and 15.

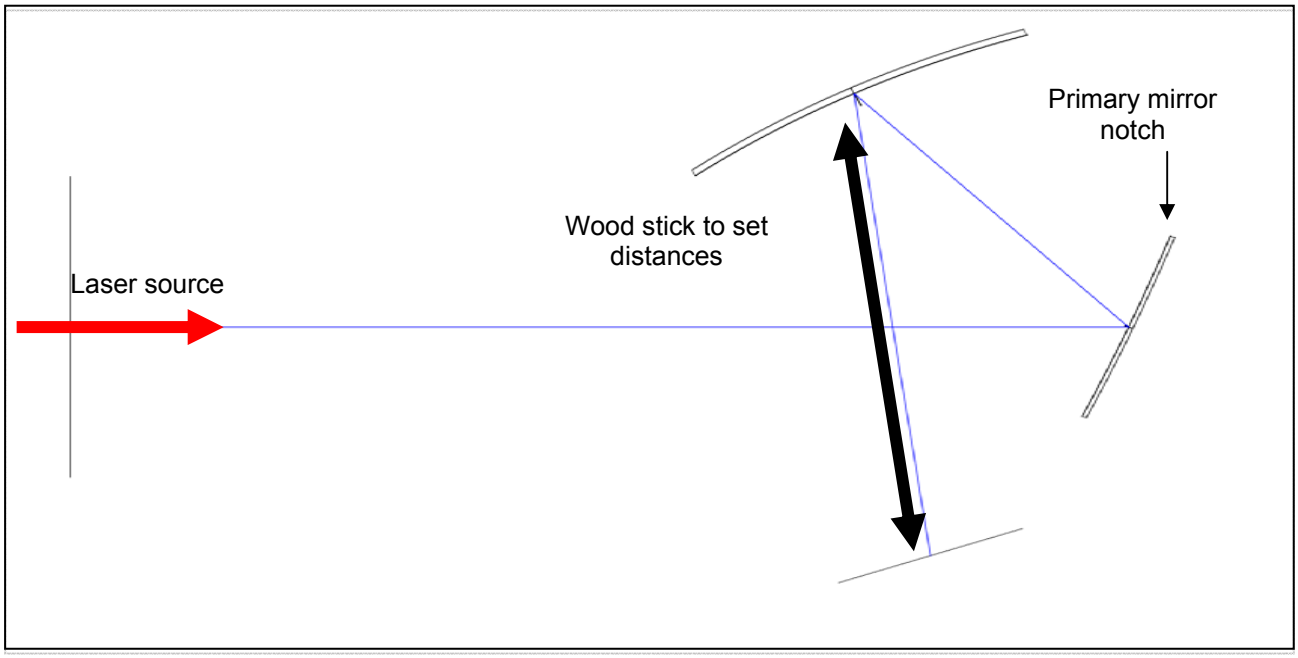

Fig 14: Preliminary alignment strategy

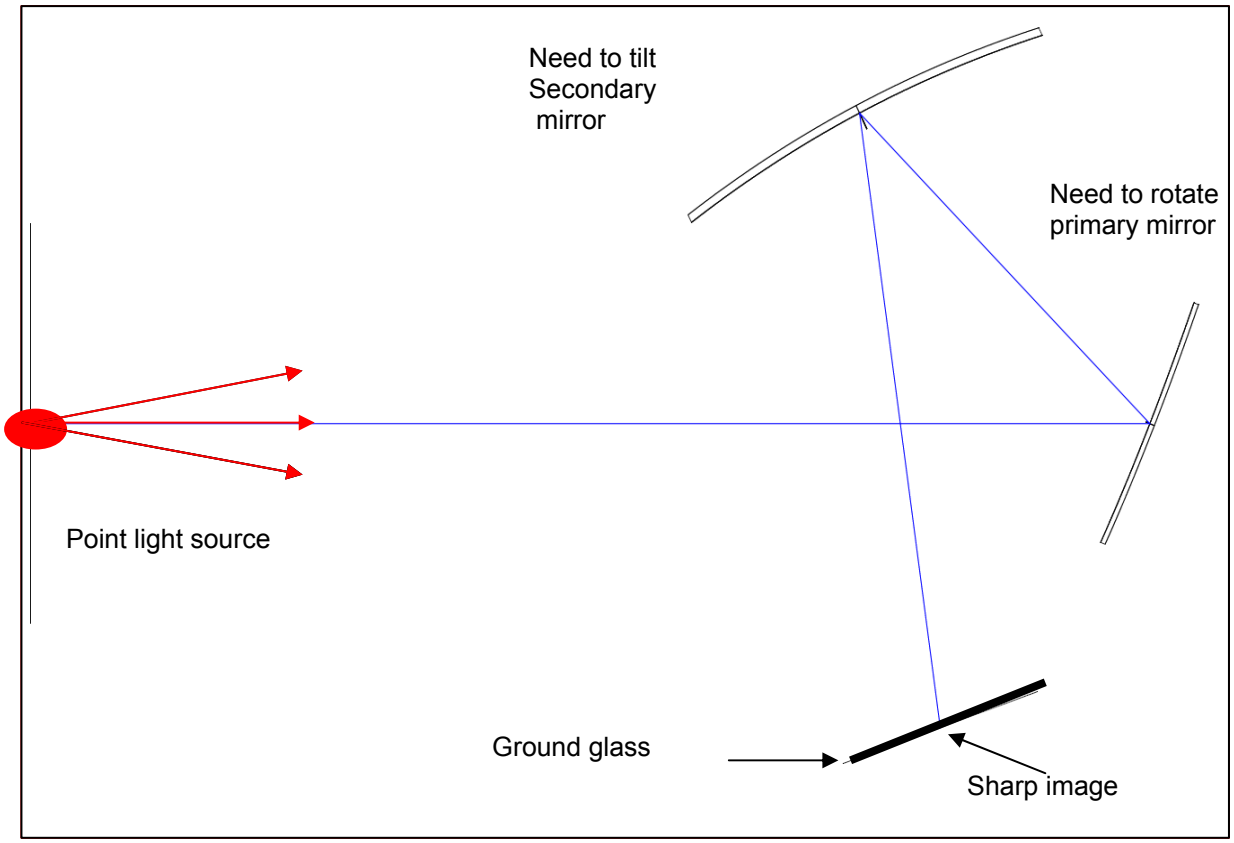

Fig 15: Final alignment strategy

Aim 2: To use breast phantoms to test feasibility and performance of the high-resolution, large field of view ultrasound breast imager

Task 6: Perform resolution, noise contrast studies
6.a. Perform resolution studies (U of C; mos. 13-15)
6.b. Perform noise/contrast stuies (U of C; mos. 13-15)

Task 7: Perform phantom measurements
7.a. Image CIRS breast phantoms (U of C; mos. 16-18)
7.b Image CIRS custom phantoms (U of C; mos. 16-18)
7.c. Image CIRS custom phantom with anatomical background (U of C; mos. 16-18)

Task 8: Refine and adjust system
8.a. Refine and adjust system in response to phantom experiments (U of C and Santec; mos. 19-24)
8.b Repeat phantom measurements and continue refining (U of C and Santec; mos. 19-24)

All of these tasks associated with Aim 2 have been deferred into the no-cost extension year 3 since they involve testing on the completed system.

KEY RESEARCH ACCOMPLISHMENTS:

- Successful simulation and construction of acoustic field of multielement sound source.
- Successful construction of 2-inch acousto optic (AO) sensor.
- Measurement of noise and spatial resolution properties of AO sensor coupled with existing video camera.
- Development and characterization of multiple acoustic lens systems, resulting in a very original acoustic-mirror design that should minimize acoustic attenuation relative to the original refraction-based designs.
- Analysis of potential for multi-frequency acquisition technique to determine lesion type and size.
- Fabrication of lenses.
- Fabrication of tank.
- Design of lens mounts and focusing system.
- Beginning assembly of complete system.

REPORTABLE OUTCOMES:

- Poster presentation: *J.R. Rosenfield, J.S. Sandhu, J.K. Tawiah, and P.J. La Rivière,* "Evaluation of the Spatial Resolution and Noise Properties of a Prototype Transmission Ultrasound Breast Imaging System Employing an Acousto-Optic Detector," NIH NIBIB training grant symposium, June, 2012.
- Oral presentation: *J.R. Rosenfield, J.S. Sandhu, J.K. Tawiah, and P.J. La Rivière,* "Evaluation of the Spatial Resolution and Noise Properties of a Prototype Transmission Ultrasound Imaging System Employing An Acousto-Optic (AO) Detector," AAPM Annual Meeting, July, 2012.
- Oral presentation, *J.R. Rosenfield, J.S. Sandhu, and P.J. La Rivière,* "Using Monochromatic Sources to Obtain Depth Information in Multispectral Transmission Ultrasound Breast Imaging,"AAPM Annual Meeting, August, 2013.

CONCLUSION:

Year 1: In summary, we have made excellent progress through the year. The simulation and construction of the sound sources and AO sensors have gone according to schedule and careful measurements have shown that the system resolution of the AO sensor coupled with the current video sensor is ~400 microns. The noise present in the imaging system is primarily electrical in nature, as evidenced by the $1/f$ noise behavior observed in the system NPS in both the x- and y-spatial directions. Our initial lens design proved impractical because of the large acoustic attenuation of the materials needed to achieve

the design, but we have produced a strong alternative design based on the use of acoustic mirrors. Fabrication is going well and should be complete this summer. Integration and testing of the complete system will then proceed as originally planned.

Year 2: We fell much further behind schedule this year due to delays in receipt of the lenses and delays involved in designing and fabricating appropriate adjustable mounts that allow for rotation, tilt, and translation. We are very close to having a complete system now which will allow for final testing in the no-cost extension period. We also explored a new direction related to using multi-frequency acquisitions to characterize lesion size.

REFERENCES:

[1] S. E. Reichenbach, S. K. Park, and R. Narayanswamy, "Characterizing digital image acquisition devices," Opt. Eng. (Bellingham) **30**, 170–177 (1991).

[2] J.M. Boone and J. A. Seibert, “An analytical edge spread function model for computer fitting and subsequent calculation of the LSF and MTF,”Med Phys. 21, 1541-1545 (1994).